Angewandte Chemie
Eine Zeitschrift der Gesellschaft Deutscher Chemiker

Supporting Information

# Cytochrome-P450-Induced Ordering of Microsomal Membranes Modulates Affinity for Drugs

*Carlo Barnaba, Bikash Ranjan Sahoo, Thirupathi Ravula, Ilce G. Medina-Meza, Sang-Choul Im, G. M. Anantharamaiah, Lucy Waskell, and Ayyalusamy Ramamoorthy**

ange_201713167_sm_miscellaneous_information.pdf

# Supplemental Information

**Table of content:**

## Experimental section

**Materials and Reagents.** Phosphate buffer components (potassium phosphate monobasic and dibasic) were purchased from Sigma-Aldrich (St. Louis, MO). 1-palmitoyl-2-oleoyl-sn-glycero-3-phosphocholine (POPC), 1-palmitoyl-2-oleoyl-sn-glycero-3-phospho-L-serine (sodium salt) (POPS), 1-palmitoyl-2-oleoyl-sn-glycero-3-phosphoethanolamine (POPE), L-α-phosphatidylinositol (sodium salt) (PI), sphingomyelin (SM, brain porcine), and cholesterol (Chol) were purchased from Avanti Polar Lipids, Inc. (Alabaster, AL). The amino acid sequence of the 4F peptide used to prepare lipid nanodiscs was **DWFKAFYDKVAEKFKEAF.** Deuterium oxide was purchased from Cambridge Isotope Laboratories (Tewksbury, MA). The 5-mm symmetrical $D_2O$-matched Shigemi NMR microtubes were purchased from Shigemi, Inc (Allison Park, PA). The silylating mixture for cholesterol methyl-esterification was prepared with pyridine, hexamethyldisilazane (HMDS) and trimethylchlorosilane (TMCS), all supplied by Sigma (St. Louis, MO, USA); the mixture was prepared using proportions of 5:2:1 (v/v/v).

**Proteins expression and purification.** Full-length wild-type cytochrome P450 2B4 (CYP2B4) and cytochrome $b_5$ (cyt$b_5$) were expressed and purified as described previously.[1, 2] The purity of CYP2B4 and cyt$b_5$ was >95% as determined by SDS−PAGE analysis. P450 concentration was determined by absorbance at 450 nm using an extinction coefficient of 91 $mM^{-1}cm^{-1}$ for the CO bound protein. Cyt$b_5$ concentration was determined by the spectrophotometric assay described elsewhere.[2]

**4F-nanodiscs preparation and characterization.** The following protocol was applied for both 4F-ER and 4F-POPC nanodiscs. The ER mixture in this study was designed according to the average composition of the smooth ER as reported by several authors.[3] Lipid powders were dissolved in HPLC-grade chloroform to make stock solutions at 20 mg/mL. The 4F peptide was

dissolved in buffer A (40 mM potassium phosphate, pH 7.4) to make a stock solution at 10mg/mL. An aliquot of the dissolved lipids was transferred to an Eppendorf vial and dried under gentle flow of $N_2$ for 3h, followed by a 2h drying step in a desiccator under vacuum. The lipid cake was hydrated with buffer A to get a 10 mg/mL solution and 4F peptide solution was added to a peptide:lipid ratio of 1:0.75 w/w (4F-ER) or 1:0.8 w/w (4F-POPC). The mixture was incubated at 37 °C o/n in slow agitation mode. Empty nanodiscs were purified by size exclusion chromatography (SEC). A Superdex 200 Increase 300/10 GL column was operated on an AKTA purifier (GE Healthcare, Freiburg, Germany). ND characterization was also performed by dynamic light scattering (DLS), on a DynaPro Nanostar equipment (Wyatt Technology Co., Goleta, CA). Correlation functions were fitted using the isotropic sphere model; fittings were performed using the software provided by the supplier (Wyatt Technology Co., Goleta, CA).

**Transmission electron microscopy.** Purified 4F-ER nanodiscs were adsorbed onto freshly glow-discharged, 300-mesh formvar/carbon coated copper grids (Electron Microscopy Sciences, Hatfield, PA, USA) and negative-stained with a 1% (wt/vol in dd$H_2O$) uranyl acetate solution. Images were taken on an Jeol 1400-plus electron microscope (Microscopy and Image Analysis Laboratory, University of Michigan, Ann Arbor, MI, USA) at 80 kV.

**$^{31}$P NMR experiments.** NMR measurements were done using a triple-resonance broadband BBI probe on a Bruker 500 MHz NMR spectrometer (Bruker Corporation, Billerica, MA) operating at a $^{31}$P resonance frequency of 202 MHz. 1024 scans were acquired with an inverse-gated $^{1}$H decoupling pulse sequence, an acquisition time of 0.5 s, 12175 Hz spectral width and a recycle delay of 3 s. Chemical shifts were referenced to $H_3PO_4$ in $D_2O$ as an external standard. A 10 Hz line broadening was used in data processing. Data were processed using TopSpin software (v. 3.17, Bruker Corporation, Billerica, MA). Solution $^{31}$P-NMR spectra of 4F-ER nanodiscs were poorly

resolved, due to the large size of nanodiscs; thus, better resolution was achieved by adding sodium cholate (20 mM final concentration) to form isotropic micelles. Nanodiscs were in buffer (40 mM KPi, pH = 7.4) and 10% $D_2O$ were added before NMR data collection.

**Cholesterol separation and quantification by GC-MS.** Cholesterol was extracted with ethylacetate and silylated according to literature.[4] One µl of the silylated cholesterol was injected on a Shimadzu QP2010 Plus GC-MS (Kyoto, Japan). A fused silica column (30 m × 0.25 mm × 0.25 µm thickness) coated with 5% phenyl-polysyloxane (Phenomenex Zebron ZB-5) was used. The injector and detector were both set at 325 °C. The oven temperature was programmed from 265 to 280 °C at 0.5 °C/min, and then from 280 to 325 °C at 4 °C/min, and held at 325 °C for 15 min. Helium was used as a carrier gas at a flow rate of 2.88 mL/min; the injection volume was 1 µL, the split ratio was 1:15, and pressure was held at 75 kPa. The quantification of cholesterol was based on the response of cholesterol to the betulinol used as an internal standard.

**Fluorescence Correlation Spectroscopy (FCS).** FCS was performed to investigate the alteration of lipid ordering induced by the presence of CYP2B4 into 4F-nanodiscs. For this purpose, we used the lipid probe DiI $C_{12}$ (1,1-didodecyl-3,3,3',3'-tetra-methylindocarbocyanine perchlorate, Figure S2a) (a kind gift of Prof. Sara Veatch Lab at the University of Michigan). DiI $C_{12}$ – which is poorly fluorescent in solution – has been used to study lipid phases in cell membrane and biomimetics.[5] In a homogeneous nanodiscs sample, the probe will be equally distributed among nanodiscs. If the addition of the protein in a fraction of the nanodiscs alters the lipid ordering, the dye would possibly partition differently, and this will be reflected in the autocorrelation function measured by FCS. 4F-ER and 4F-POPC nanodiscs were prepared and purified as described above, in 40 mM KPi pH 7.4 buffer. Following SEC purification, an equimolar amount of the fluorescent probe DiI $C_{12}$ was added. After the addition of the probe, the empty nanodiscs were incubated 2h at room

temperature, following the addition of CYP2B4. CYP2B4 was added in stoichiometric or limiting amount (1:2.5 protein:nanodiscs ratio) and the nanodiscs/protein solution was incubated overnight at room temperature. Before FCS experiment, the nanodiscs solutions were centrifuged at 10000 rpm and 4°C for 10 min to remove any aggregates. The total concentration of nanodiscs was kept constant in all the performed experiments. The nanodiscs solution was diluted to 10 nM, and FCS was performed on an Alba time-resolved confocal microscope (ISS, Inc.). A calibration curve with known concentrations of Cy3 fluorescent probe was performed to estimate the laser spread point function. Two replicates were performed for each experiment, preparing fresh 4F-nanodiscs each time; for each replicate, two FCS curves traces (5 min length) were recorded and averaged. Data were analyzed using the software PyCorrFit developed by Muller et al.[6] Autocorrelation functions were fit using a 3D-diffusion model with Gaussian laser profile by non-linear least square fitting. The goodness of fit was derived from the $\chi^2$value or residual plot.

**Differential Scanning Calorimetry (DSC).** DSC experiments were performed using a Nano DSC system (TA Instruments, New Castle, DE). CYP2B4 in solution of incorporated in 4F-ER nanodiscs, as well as empty nanodiscs were dissolved in 40 mM KPi buffer (pH 7.4). The instrument was conditioned by performing two consecutive scans with 40 mM KPi buffer alone prior to the analysis of the sample. CYP2B4 endotherms were measured by scanning sample from 15 °C to 130 °C at a scan rate of 1 °C/min. Endotherms were baseline corrected, and transition temperatures ($T_m$) and changes calorimetric enthalpies ($\Delta H_{cal}$) were determined by fitting the data using the software package Nano Analyze (TA Instruments).

**Circular Dichroism.** Circular dichroism (CD) spectroscopy was performed using a Jasco 1500 spectrophotometer (Jasco Inc., Easton, MD). The instrument was pre-equilibrated at 25°C for 10 min prior to the acquisition of data. To prevent the dynode from exceeding 700 V, CYP2B4 and

CYP2B4 in nanodiscs were diluted to a total protein concentration of 1 μM with CD buffer (10 mM KPi, pH 7.4). The sample was loaded into a 0.1 cm path length quartz cuvette and allowed to equilibrate for 5 min at 25°C inside the CD spectrophotometer prior data collection. The instrument was set to record data from 175 to 260 nm, with a scan speed of 50 nm/min and a 0.5 nm bandwidth. CD spectra were smoothed, buffer-subtracted and corrected for CYP2B4 concentration. For CYP2B4 in 4F-ER nanodiscs, we attempt to subtract the contribution of the 4F-peptide, as reported by McClary et al.[7] for MSP-based nanodiscs. However, we were unable to have consistency and reproducibility in our measurements. Thus, we decided to measure CD on CYP2B4 reconstituted in small unilamellar vesicles (SUV), which are devoid of significant absorbance in the UV region. ER SUV were prepared with sonication protocol, as described recently.[8] The secondary structural content was estimated from far-UV CD spectra recorded at 25 °C using the CDSSTR and SELCON3 routines implemented in the CDPro software package.[9]

**Spectral binding titrations.** Enzyme titrations were performed with a DeNovix DS-11 FX spectrophotometer (Wilmington, DE). Experiments were performed at room temperature, the wavelength range typically encompassed 340 to 700 nm, and the readings were taken in 1-nm steps. Binding affinities of BHT and 4-CPI with CYP2B4 were determined by titration of 1.5-2.5 μM of enzyme in soluble or nanodiscs form with the ligand, in a total volume of 0.7 ml of 40 mM KPi buffer (pH 7.4). High- and low-spin molar fraction were computed as describe previously using SpectraLab software[10]. Both ligands were dissolved in ethanol and the final concentration of solvent in the system was <1%. Spectral binding equilibrium constants ($K_S$) were estimated using OriginLab software (OriginLab Co., Northampton, MA, USA) with non-linear regression. For BHT, Michaelis-Menten hyperbolic equation was used. For 4-CPI, given its sub-micromolar affinity for the enzyme, the tight-binding model was chosen.[11]

**Template-based full-length CYP2B4 modeling.** The full-length structure of mammalian CYP2B4 was modelled by using advance modeling technique in Modeller 9.18[12] from its crystal structure (PDB ID: 1SUO).[13] The missing coordinates of N-terminal transmembrane (TM) domain spanning residues 1 to 27 were assigned using multiple templates (PDB IDs: 2MJ2, 5LJ3, 1EYS and 4LXJ), and were obtained from different protein threading servers as described elsewhere.[14] The spatial coordinates for the full-length CYP2B4 were assigned using advance modeling (Modeller) by combining the CYP2B4 crystal structure (1SUO) and modeled TM domain. Next, the HEME coordinates were copied to the full-length model structure of CYP2B4 from its crystal structure (1SUO) using a local python script in Modeller.

**Molecular dynamics (MD) simulations.** The structure and dynamics of model mouse CYP2B4 was studied in different membrane systems using CHARMM36[15] (all-atom) and Martini v2.2[16] (Coarse-grained) force fields in GROMACS[17] and are listed in Table S2. Three model membranes in aqueous environment were used in the MD simulations. POPC membrane was used as control, since a previous MD study in cytochrome P450 have been performed in this system.[18] The ER membrane composition before (ER) and after lipid exchange ($ER_{ex}$) was according to Table S1 (Supplemental Information). The targeted all-atom lipid bilayers and coarse-grained (CG) membrane scaffold protein encased nanodiscs were generated using CHARMM_GUI.[19] All lipid-bilayers/nanodiscs were subjected to pre-equilibration followed by substantial production MD simulation. The water thickness in lipid bilayer was extended in the z-dimension to sufficiently embed the CYP2B4 model structure using *g_membed* program as described elsewhere.[20] The protein was embedded using the INSANE python program in the CG-MD simulation systems. The MD parameters were referenced from our previous studies.[21] The all-atom and CG-MD MD systems were simulated for 100 ns and 10 μs, respectively. The temperature coupling of protein

and solvent was at 310 K, and a temperature above the phase transition temperature of targeted lipids was considered. The MD trajectory analysis were executed using Gromacs and VMD programs. All MD simulations were carried out using Gromacs v 5.0.7 running parallel in *SGI-uv* cluster equipped with 256 cores at Institute for Protein Research, Osaka University, Japan.

**Statistical analysis.** Means and standard deviations were calculated using OriginPro v.2017 (OriginLab Co., Northampton, MA). One-way ANOVA was performed to statistically evaluate the change in phospholipid content in the P450- and $b_5$-incorporated nanodiscs compared to the ER membrane. Tukey's honest significant multiple comparison was used to determine statistical differences between samples at a 95% confidence level ($p \leq 0.05$). The 2D graphs from MD trajectory analysis were generated using Grace (http://plasma-gate.weizmann.ac.il/Grace/).

**References**:


[1] S. Ahuja, N. Jahr, S.-C. Im, S. Vivekanandan, N. Popovych, S. V. Le Clair, R. Huang, R. Soong, J. Xu, K. Yamamoto, *Journal of Biological Chemistry* **2013**, *288*, 22080-22095; A. S. Saribas, L. Gruenke, L. Waskell, *Protein expression and purification* **2001**, *21*, 303-309.

[2] H. Zhang, S. C. Im, L. Waskell, *J Biol Chem* **2007**, *282*, 29766-29776.

[3] L. Brignac-Huber, J. R. Reed, W. L. Backes, *Molecular pharmacology* **2011**, *79*, 549-557; C. Barnaba, M. J. Martinez, E. Taylor, A. O. Barden, J. A. Brozik, *J Am Chem Soc* **2017**, *139*, 5420-5430.

[4] C. Barnaba, M. T. Rodriguez-Estrada, G. Lercker, H. S. Garcia, I. G. Medina-Meza, *Steroids* **2016**, *116*, 52-59.

[5] M. B. Stone, S. A. Shelby, M. F. Núñez, K. Wisser, S. L. Veatch, *eLife* **2017**, *6*, e19891; A. S. Klymchenko, R. Kreder, *Chemistry & biology* **2014**, *21*, 97-113.

[6] P. Muller, P. Schwille, T. Weidemann, *Bioinformatics* **2014**, *30*, 2532-2533.

[7] W. D. McClary, J. P. Sumida, M. Scian, L. Paço, W. M. Atkins, *Biochemistry* **2016**, *55*, 6258.

[8] C. Barnaba, M. J. Martinez, E. Taylor, A. O. Barden, J. A. Brozik, *Journal of the American Chemical Society* **2017**.

[9] N. Sreerama, R. W. Woody, *Analytical biochemistry* **2000**, *287*, 252-260.

[10] J.-P. Renaud, D. R. Davydov, K. P. Heirwegh, D. Mansuy, *Biochemical Journal* **1996**, *319*, 675-681.

[11] I. H. Segel, *Enzyme kinetics, Vol. 360*, Wiley, New York, **1975**.

[12] A. Šali, T. L. Blundell, *Journal of molecular biology* **1993**, *234*, 779-815.

[13] E. E. Scott, M. A. White, Y. A. He, E. F. Johnson, C. D. Stout, J. R. Halpert, *Journal of Biological Chemistry* **2004**, *279*, 27294-27301.

[14] B. R. Sahoo, J. Maharana, G. K. Bhoi, S. K. Lenka, M. C. Patra, M. R. Dikhit, P. K. Dubey, S. K. Pradhan, B. K. Behera, *Molecular BioSystems* **2014**, *10*, 1104-1116.

[15] J. B. Klauda, R. M. Venable, J. A. Freites, J. W. O'Connor, D. J. Tobias, C. Mondragon-Ramirez, I. Vorobyov, A. D. MacKerell Jr, R. W. Pastor, *The journal of physical chemistry B* **2010**, *114*, 7830-7843.

[16] S. J. Marrink, H. J. Risselada, S. Yefimov, D. P. Tieleman, A. H. De Vries, *The journal of physical chemistry B* **2007**, *111*, 7812-7824.

[17] D. Van Der Spoel, E. Lindahl, B. Hess, G. Groenhof, A. E. Mark, H. J. Berendsen, *Journal of computational chemistry* **2005**, *26*, 1701-1718.

[18] I. G. Denisov, A. Y. Shih, S. G. Sligar, *Journal of Inorganic Biochemistry* **2012**, *108*, 150-158.

[19] E. L. Wu, X. Cheng, S. Jo, H. Rui, K. C. Song, E. M. Dávila-Contreras, Y. Qi, J. Lee, V. Monje-Galvan, R. M. Venable, *Journal of computational chemistry* **2014**, *35*, 1997-2004.

[20] B. R. Sahoo, T. Fujiwara, *Molecular BioSystems* **2017**, *13*, 193-207.

[21] B. R. Sahoo, T. Fujiwara, *PloS one* **2016**, *11*, e0158702; B. R. Sahoo, K. Maruyama, J. R. Edula, T. Tougan, Y. Lin, Y.-H. Lee, T. Horii, T. Fujiwara, *Scientific Reports* **2017**, *7*.

**Acronyms and Abbreviations**

| | |
|---|---|
| 4-CPI | 4-(4-chlorophenyl)imidazole |
| BHT | Butylated hydroxytoluene |
| CD | Circular Dichroism |
| Chol | Cholesterol |
| CYP2B4 | Cytochrome P450 2B4 |
| Cyt$b_5$ | Cytochrome $b_5$ |
| DiI $C_{12}$ | 1,1-didodecyl-3,3,3',3'-tetra-methylindocarbocyanine perchlorate |
| DLS | Dynamic Light Scattering |
| DRM | Detergent Resistant Microdomains |
| DSC | Differential Scanning Calorimetry |
| ER | Endoplasmic reticulum |
| $ER_{ex}$ | Endoplasmic reticulum after lipid exchange |
| FCS | Fluorescence Correlation Spectroscopy |
| GC-MS | Gas-chromatography Mass-Spectrometry |
| $K_S$ | Spectral binding equilibrium constant |
| NMR | Nuclear Magnetic Resonance |
| PI | L-α-phosphatidylinositol |
| POPC | 1-palmitoyl-2-oleoyl-sn-glycero-3-phosphocholine |
| POPE | 1-palmitoyl-2-oleoyl-sn-glycero-3-phosphoethanolamine |
| POPS | 1-palmitoyl-2-oleoyl-sn-glycero-3-phospho-L-serine (sodium salt) |
| RMS | Root Mean Square |
| RMSD | Root Mean Square Deviation |
| SEC | Size-exclusion chromatography |
| SM | Sphyngomyelin |
| SUV | Small Unilamellar Vesicles |
| TEM | Transmission Electron Microscopy |
| TMD | Transmembrane domain |

**Table S1.** Percentage composition of the ER biomimetic used for the MD simulations before (ER) and after ($ER_{ex}$) lipid exchange.

| Lipid | ER | $ER_{ex}$ |
|---|---|---|
| **POPC** | 58 | 54 |
| **POPS** | 7 | 6 |
| **POPE** | 20 | 8 |
| **PI** | 7 | 8 |
| **SM** | 4 | 17 |
| **Cholesterol** | 4 | 7 |

**Table S2.** Autocorrelation parameters obtained with fluorescence correlation experiments in 4F-ER and 4F-POPC nanodiscs with and without CYP2B4, in the presence of stoichiometric amounts of DiI $C_{12}$ lipid probe. $\tau_D$ = diffusion correlation time (ms); N = average number of molecule in the considered volume; D = diffusion coefficient ($10^{-8}$ $cm^{-2}$ $s^{-1}$).

| Sample | $\tau_D$ | N | D |
|---|---|---|---|
| ***4F-ER (empty)*** | 1.3 ± 0.1 | 2.5 ± 0.3 | 6.6 |
| ***4F-ER:CYP2B4 2.5:1*** | 1.6 ± 0.2 | 0.8 ± 0.2[†] | 7.2 |
| ***4F-ER:CYP2B4 1:1*** | 1.0 ± 0.2 | 1.4 ± 0.1 | 8.6 |
| ***4F-POPC (empty)*** | 1.2 ± 0.1 | 2.1 ± 0.5 | 5.4 |
| ***4F-POPC:CYP2B4 2.5:1*** | 2.6 ± 0.8 | 2.3 ± 1.4 | 3.3 |
| ***4F-POPC:CYP2B4 1:1*** | 1.5 ± 0.1 | 4.1 ± 0.9 | 5.7 |

[†] *p = 0.067*

**Table S3.** Summary of all-atom and coarse-grained MD simulation parameters for full-length CYP2B4 binding to lipid membrane systems.

| Simulation System | Force field | Lipid number | Solvent | MSP | Time (ns) |
|---|---|---|---|---|---|
| **All-atom MD systems** | | | | | |
| CYP2B4 + POPC | CHARMM36 | 200 | 14326 | | 100 |
| CYP2B4 + ER | CHARMM36 | 200 | 18568 | | 100 |
| CYP2B4 + $ER_{ex}$ | CHARMM36 | 200 | 21306 | | 100 |
| **Coarse-grained MD systems** | | | | | |
| CYP2B4 + POPC | Martini v2.2 | 200 | 42440 | 2 | 10000 |
| CYP2B4 + ER | Martini v2.2 | 200 | 42329 | 2 | 10000 |
| CYP2B4 + $ER_{ex}$ | Martini v2.2 | 200 | 41286 | 2 | 10000 |

ER: Endoplasmic reticulum; $ER_{ex}$: Endoplasmic reticulum after lipid exchange (see Table S1)

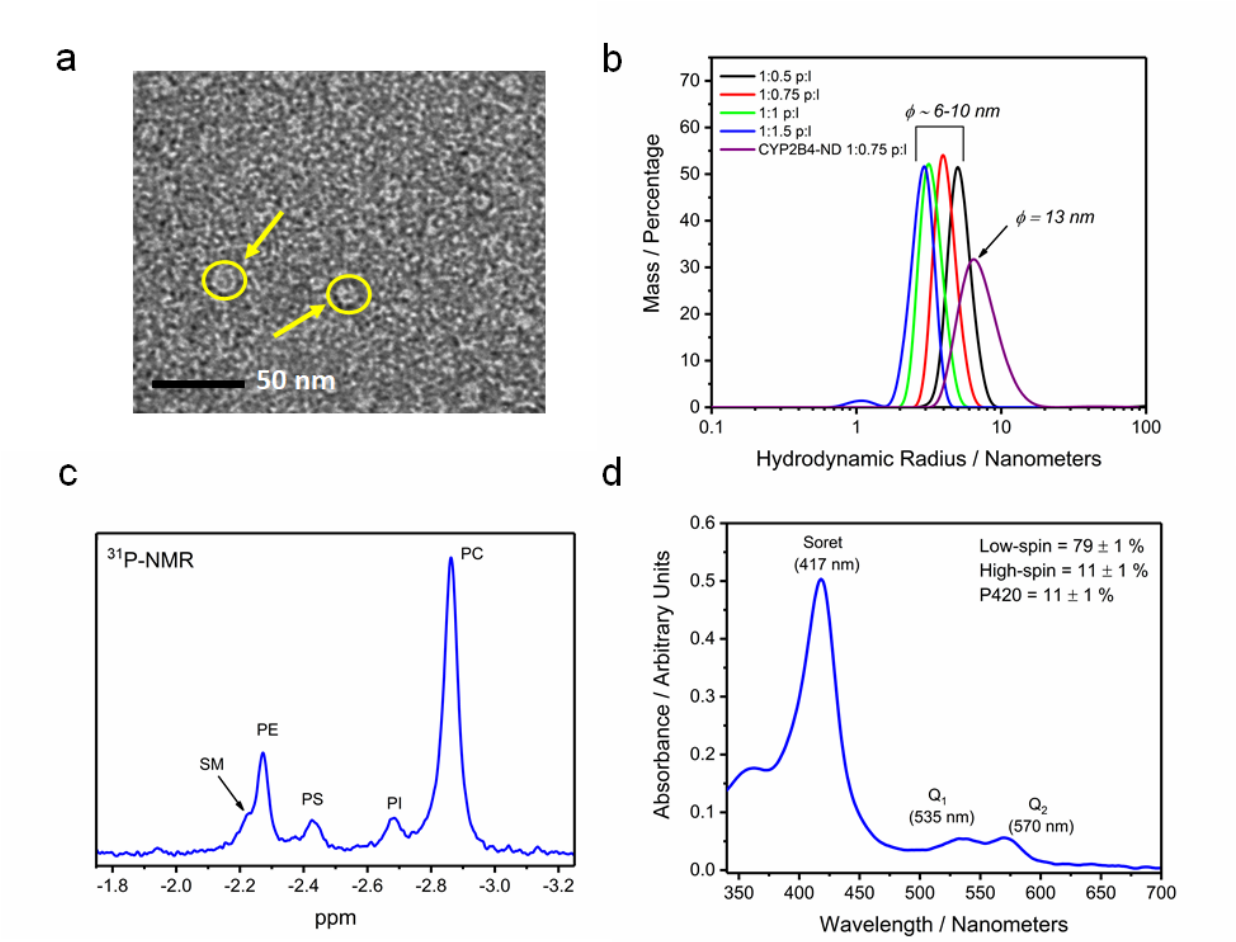


**Figure S1. A biomimetic of the endoplasmic reticulum membrane at nanometer scale. (a)** 4F-peptide is able to trap a lipid membrane patch, forming round shaped nanodiscs, as unveiled by TEM imaging; **(b)** varying the peptide to lipid ratio, it is possible to form nanodiscs up to 13-15 nm diameter, as measured by dynamic light scattering; larger nanodiscs can potentially be used for the incorporation of protein complexes in a near native environment. **(c)** $^{31}$P-NMR in detergent-solubilized 4F-ER nanodiscs show retention of the lipid composition, which consisted in several phospholipids and cholesterol. **(d)** Cytochrome P450 2B4 is not interacting with the lipid components at the heme prosthetic group: the visible spectra of the Soret and Q-band regions show absence of ligand-induced high-spin shifts, being the high-to-low spin ratio analogue to membrane-free CYP2B4.

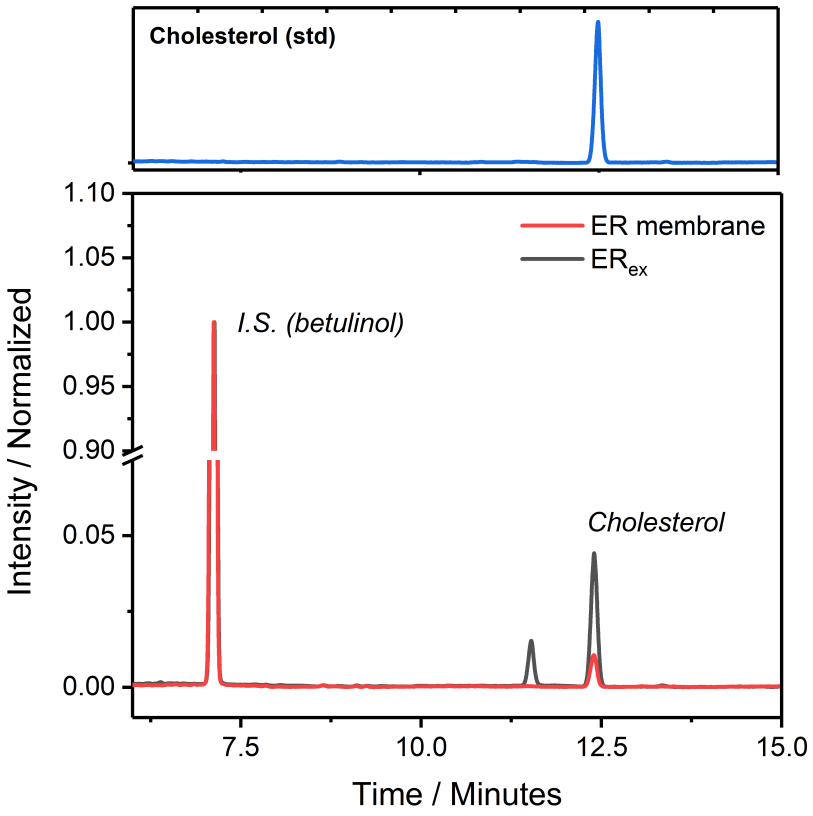


**Figure S2.** Gas-chromatogram for cholesterol quantification in ER nanodiscs (ER) and in CYP2B4-containing nanodiscs after the lipid-exchange experiment ($ER_{ex}$). The traces were normalized to the internal standard betulinol (I.S.). The chromatogram of pure cholesterol is shown in the upper panel.

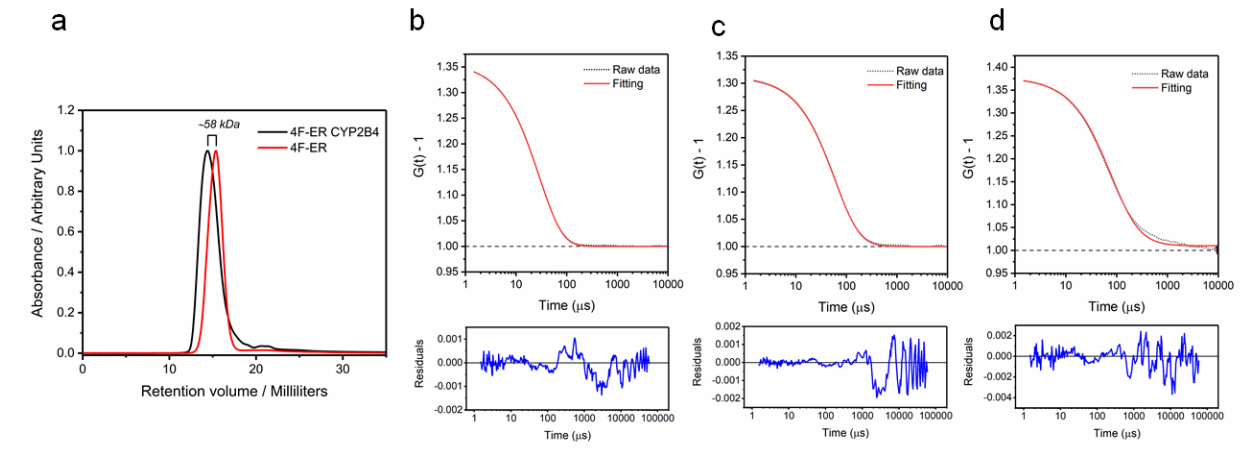


**Figure S3.** Formation of 4F-ER nanodiscs. a) Size-exclusion chromatography of empty 4F-ER and 4F-ER nanodiscs incorporated with CYP2B4. Dynamic Light Scattering autocorrelation function for 4F-ER nanodiscs. b) Empty 4F-ER nanodiscs; c) CYP2B4 4F-ER nanodiscs; d) CYP2B4 4F-ER nanodiscs after lipid exchange. Autocorrelation functions were fitted to a 3D diffusion model. Residuals of the fittings are depicted in the bottom for each measurement.

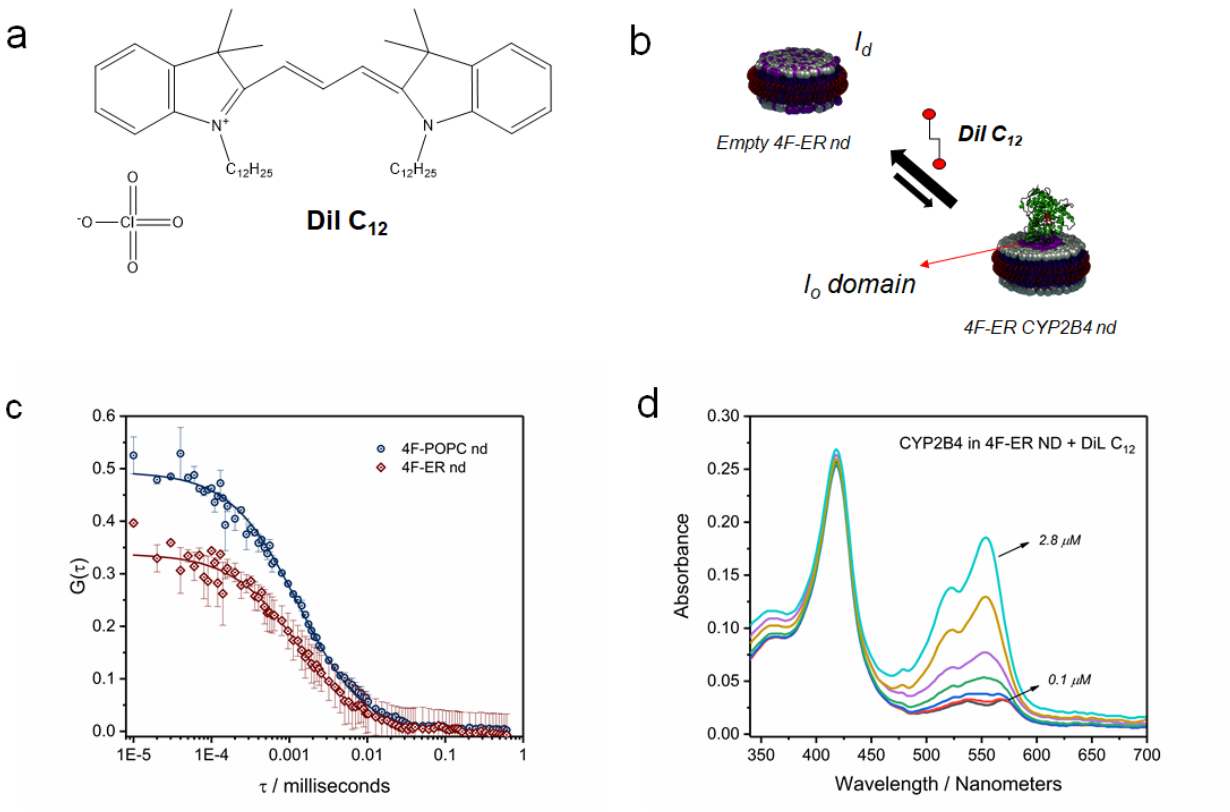


**Figure S4.** a) Structure of the fluorescent lipid probe DiI $C_{12}$. b) Schematic of the FCS experiment used to assess the formation of liquid-ordered regions in CYP2B4 4F-ER nanodiscs. The lipid-probe DiI $C_{12}$ differently partitioned onto P450-containing nanodiscs, causing changes in the autocorrelation function. c) FCS autocorrelation function for empty 4F-ER and 4F-POPC nanodiscs containing stoichiometric amount of DiI $C_{12}$, showing slight difference in the distribution of the lipid probe. Data were fitted with a 3D Gaussian model (see Experimental Section for details about the fitting procedure). d) UV-Vis titration of CYP2B4 with the lipid probe DiI $C_{12}$. The Soret region of the heme (390-420 nm) is not altered by the addition of the dye, indicating no interaction with the active site of the cytochrome P450. DiI $C_{12}$ absorbs in the 500-600 nm region.

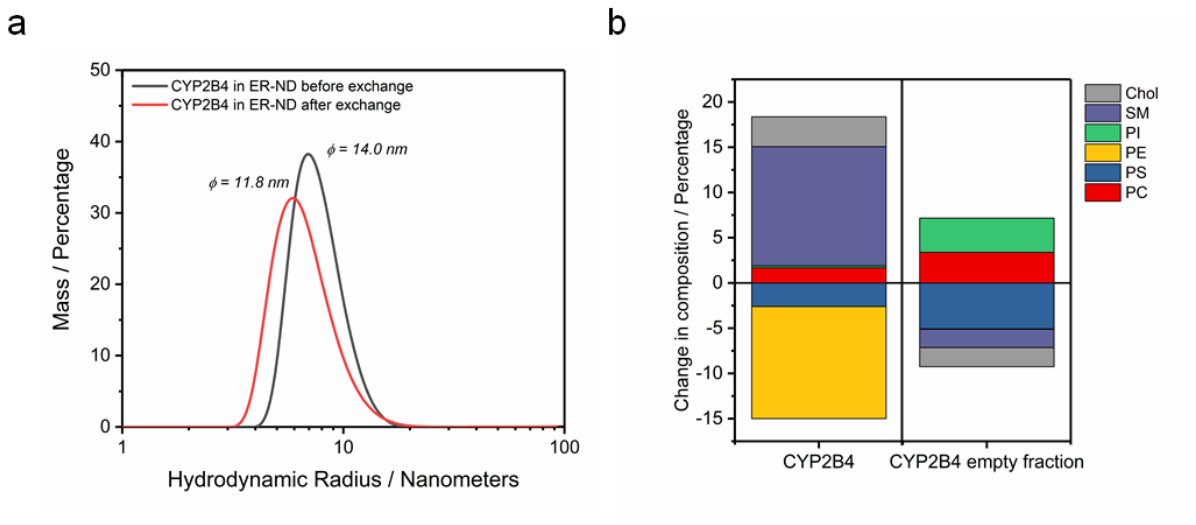


**Figure S5.** a) DLS profiles of CYP2B4 4F-ER nanodiscs before (solid black line) and after (solid red line) lipid exchange, showing reduction in the nanodiscs size. b) Change in composition in respect to the initial ER mixture in 4F-ER CYP2B4 nanodiscs after exchange (left), and in the corresponding empty nanodiscs fraction. The empty fractions are partially depleted of SM and cholesterol.

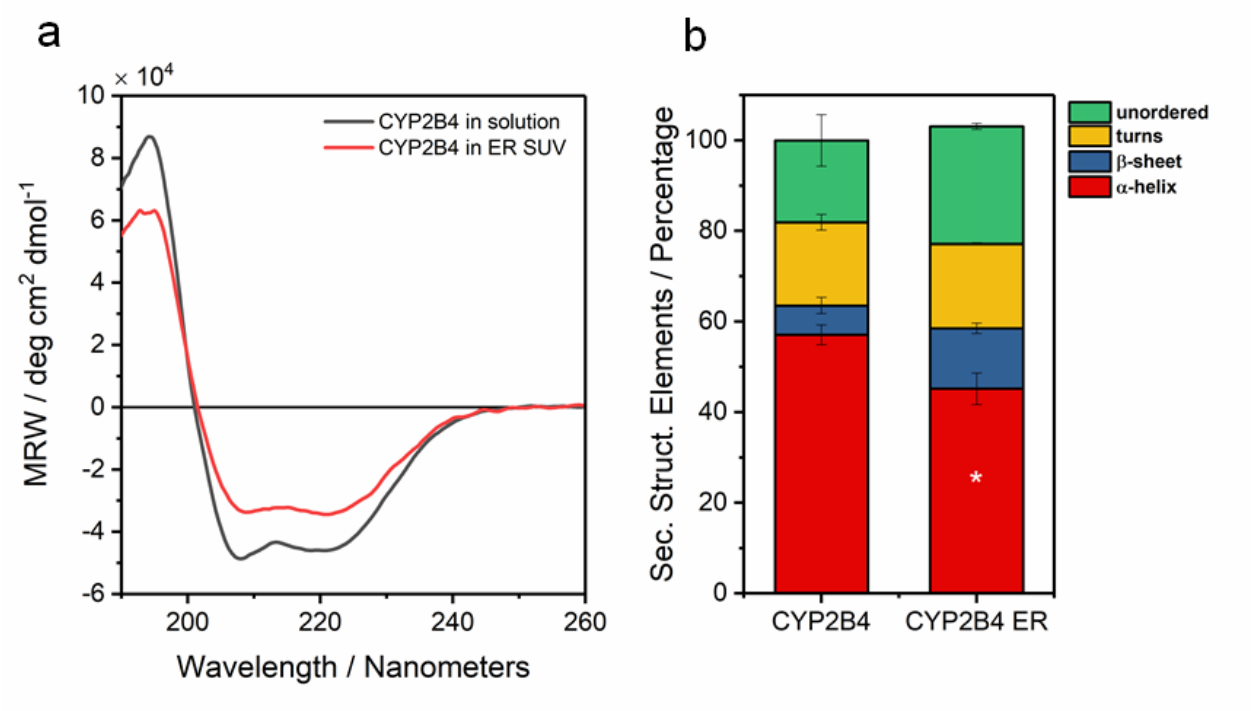


**Figure S6.** a) Circular dichroism of CYP2B4 in solution (solid black line) and ER SUV (solid red line). Absorbance "flattening" due to SUV heterogeneity was observed. b) Percentage of secondary structure elements as calculated using the CDPro software. Only a small change of α-helix/β-sheet ratio is observed, as computed by the SELCON3 algorithm (see Experimental Section for further details). * $p < 0.05$.

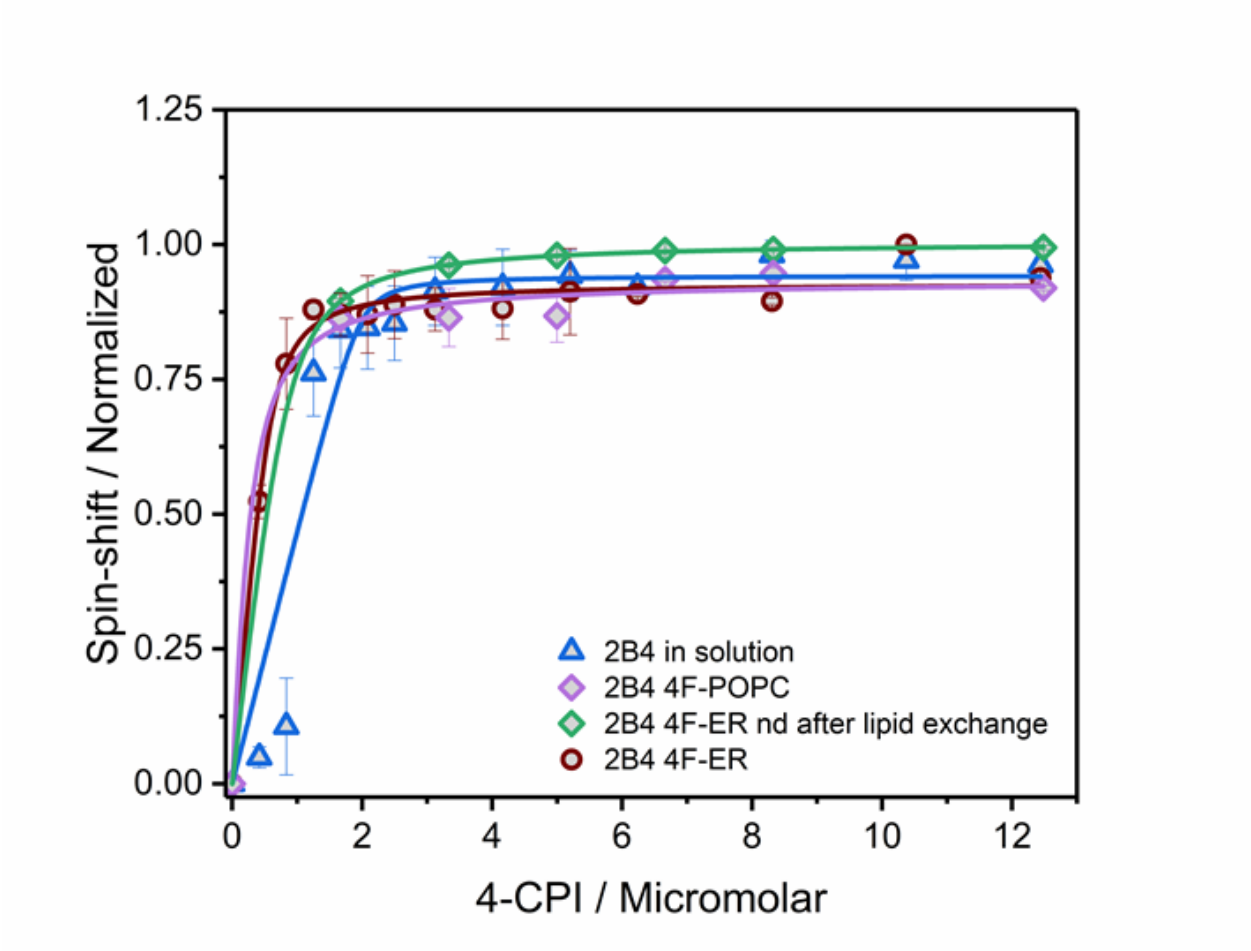


**Figure S7.** UV-Vis titration of CYP2B4 with the compound 4-CPI in solution and several nanodiscs preparations. The concentration-dependent of the overall spin shift variation was fitted with Hill's equation (see the Experimental Section for further details).

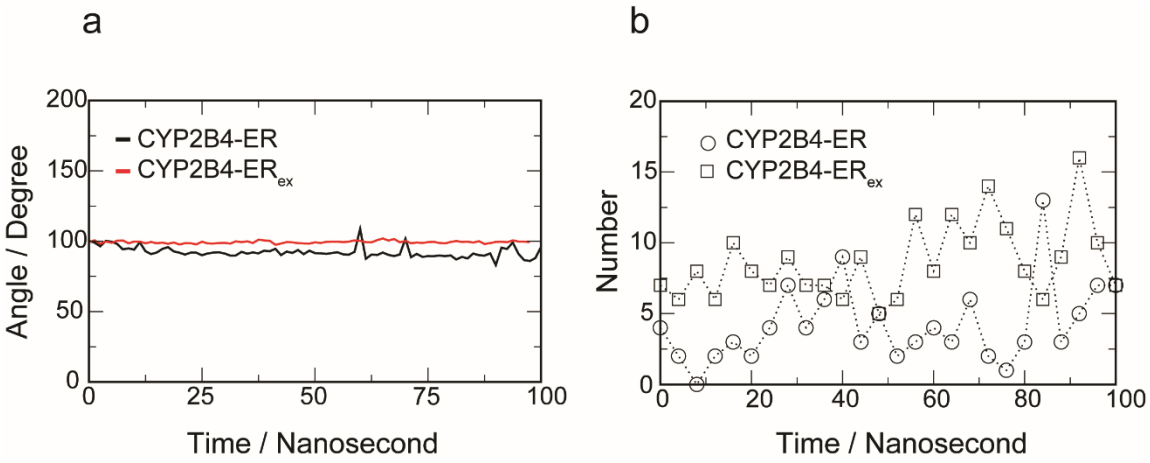


**Figure S8.** a) Graph shows the TMD helix angle per residues w.r.t. simulation time. An ideal α-helix shows 100 º helix angle per residues. b) Hydrogen bond plots between CYP2B4 and ER membrane lipids during the 100 ns of simulation.

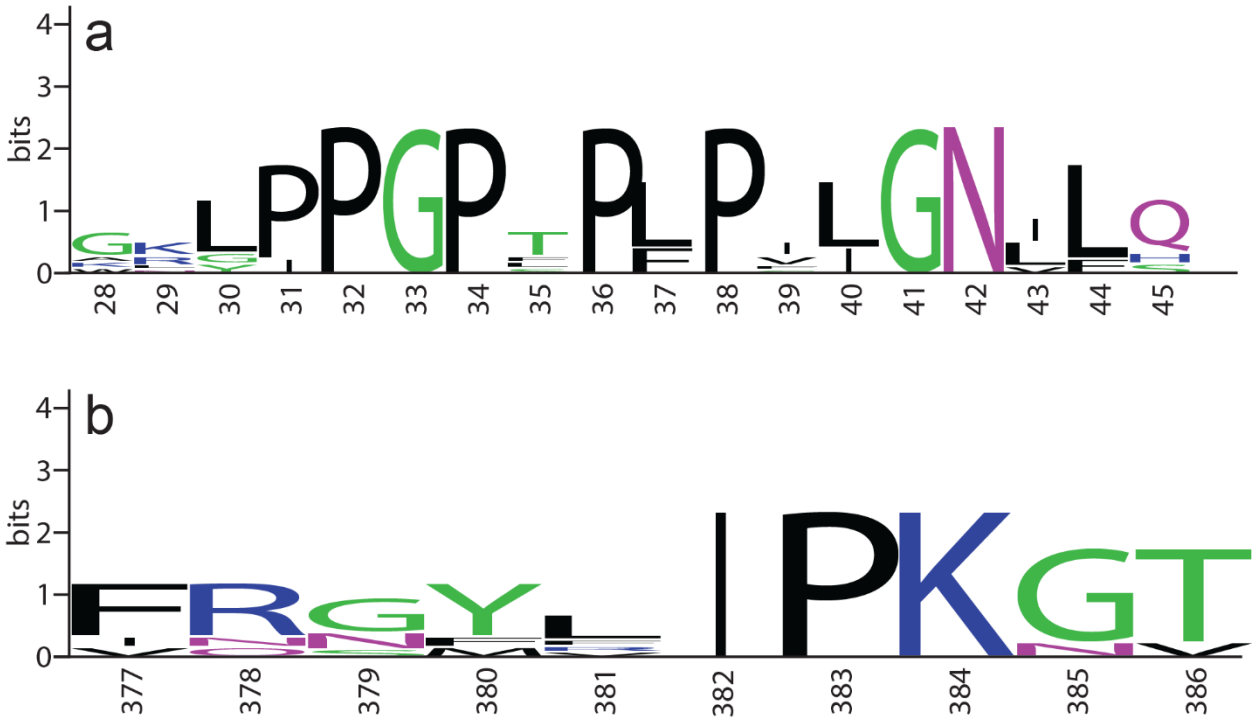


**Figure S9.** SM-binding residues determined by MD simulations on ER lipid membranes are conserved along microsomal P450s. Sequence logos of the residues constituting the TM-connecting loop (a) and the β-finger in several microsomal P450s (2B4, 2C1, 2C2, 2C9, 2C19, 2D6, 2E1, 3A4, 3A5, 4F8, 4A11). Position labels were based on the sequence of CYP2B4. The figure was generated by WebLogo 3 (http://weblogo.threeplusone.com)